On the magnetic, electrical and thermodynamic properties of Ce_3NiGe_2

2003 J. Phys.: Condens. Matter 15 8837

(http://iopscience.iop.org/0953-8984/15/50/015)

INSTITUTE OF PHYSICS PUBLISHING JOURNAL OF PHYSICS: CONDENSED MATTER

J. Phys.: Condens. Matter **15** (2003) 8837–8851 PII: S0953-8984(03)68636-4

On the magnetic, electrical and thermodynamic properties of Ce_3NiGe_2

A P Pikul[1,5], D Kaczorowski[1], H Michor[2], P Rogl[3], E Bauer[2], G Hilscher[2] and Yu Grin[4]

[1] Institute of Low Temperature and Structure Research, Polish Academy of Sciences, PO Box 1410, 50-950 Wrocław, Poland
[2] Institut für Festkörperphysik, Technische Universität Wien, Wiedner Hauptstraße 8–10, 1040 Wien, Austria
[3] Institut für Physikalische Chemie, Universität Wien, Währinger Straße 42, 1090 Wien, Austria
[4] Max-Planck-Institut für Chemische Physik Fester Stoffe, Nöthnitzer Straße 40, 01187 Dresden, Germany

E-mail: A.Pikul@int.pan.wroc.pl

Received 5 September 2003
Published 3 December 2003
Online at stacks.iop.org/JPhysCM/15/8837

Abstract

Ce_3NiGe_2 was studied by means of DC and AC magnetic susceptibility, magnetization, electrical resistivity, magnetoresistivity and specific heat measurements. The compound undergoes two subsequent magnetic phase transitions at $T_N = 6.2$ K and $T_1 = 5.2$ K, from paramagnetic to antiferromagnetic and to ferromagnetic-like ground state, respectively. The electrical and thermodynamic behaviour is governed by interplay of RKKY, Kondo and crystal field interactions, with the Kondo temperature of the order of 10 K and the total crystal–field splitting of about 690 K.

1. Introduction

Ternary cerium compounds with d-electron transition metals and p-electron metalloids have attracted much interest in recent decades because of their remarkable physical properties, that are mainly governed by hybridization of 4f electronic states with the conduction band. The recent discovery of pressure-induced superconductivity in a non-Fermi-liquid system $CeNi_2Ge_2$ [1, 2] has motivated systematic experimental studies on other phases from the Ce–Ni–Ge system. In the course of these investigations it was established that the physical behaviour of compounds such as $CeNiGe_2$, $CeNiGe_3$ and $Ce_2Ni_3Ge_5$ is governed by interplay of magnetic exchange, Kondo and crystal field interactions [3–8]. At low temperatures all these ternaries exhibit multiple phase transitions of antiferromagnetic character and show moderately enhanced electronic specific heat. The resistivity is dominated by a strong Kondo

[5] Author to whom any correspondence should be addressed.

effect. Their magnetic and electrical transport properties are highly anisotropic in both ordered and paramagnetic regions.

In this paper we report on Ce_3NiGe_2, another ternary compound from the Ce–Ni–Ge system. To the best of our knowledge no information on its physical properties exists in the literature, except for our own fragmentary data published in conference articles [9–11]. We should note however that most recently an independent study on Ce_3NiGe_2 has been performed at the University of Bordeaux and the interested reader is referred to the thesis by Durivault [12].

2. Experimental details

Polycrystalline samples of Ce_3NiGe_2 and La_3NiGe_2 were prepared by arc-melting the stoichiometric amounts of the elemental components under argon atmosphere and subsequent annealing in vacuum at 800 °C for 1 week and at 600 °C for 2 weeks. The quality of the products was checked by powder x-ray diffraction (STOE diffractometer with Cu Kα radiation) and microprobe analysis (Philips 515 scanning electron microscope with EDAX PV 9800 spectrometer).

The DC magnetic susceptibility and magnetization were measured in the temperature range 1.7–300 K and in applied magnetic fields up to 5 T using a Quantum Design MPMS-5 SQUID magnetometer. The AC magnetic susceptibility was studied from 1.5 to 300 K and in steady magnetic fields up to 9 T employing an Oxford Instruments AC susceptometer. The probing magnetic field had amplitude up to 20 Oe and a frequency between 20 and 3000 Hz. The electrical resistivity and magnetoresistivity measurements were performed in the temperature interval 1.5–300 K and in external fields up to 14 T using a Quantum Design PPMS platform and four-point DC method. The specific heat studies were carried out in the temperature range 1.7–140 K and in magnetic fields up to 9 T employing a homemade calorimeter and adiabatic step-heating technique.

3. Results and discussion

3.1. Crystal structure of Ce_3NiGe_2

The x-ray powder diffraction patterns of Ce_3NiGe_2 and La_3NiGe_2 were easily indexed with an orthorhombic lattice. The unit cell parameters were refined using diffraction angles 2θ of 14°–100° (5°–87°) and 487 (385) reflections for the cerium (lanthanum) compound, yielding $a = 11.916(1)$ Å, $b = 4.302(1)$ Å and $c = 11.656(1)$ Å for Ce_3NiGe_2, and $a = 12.043(2)$ Å, $b = 4.352(5)$ Å and $c = 11.856(3)$ Å for La_3NiGe_2. For both compounds, the so-obtained lattice parameter values are in good agreement with the literature data [13, 14].

The crystal structure of La_3NiGe_2 was determined before [14] by means of a single-crystal x-ray diffraction experiment. Here, we refined the crystal structure of the cerium from the powder data using the Rietveld method with the FULLPROF program [15], assuming an isotropic approximation for the atomic displacement parameters. The calculations converged with the reliability factor $R_{\mathrm{Bragg}} = 0.050$, and the final values of atomic coordinates and displacement parameters are presented in table 1.

From the refinement results and in accordance with the lattice parameter ratios (a:b:c = 2.767:1:2.724 for La_3NiGe_2 and a:b:c = 2.758:1:2.698 for Ce_3NiGe_2) the structure of the cerium compound is of the La_3NiGe_2 type (see figure 1). The nickel and germanium atoms form a one-dimensional polyanion extended along the [010] direction. The polyanion contains a zigzag chain of two-bonded germanium (Ge2(2b)) and nickel atoms with the distance of 2.544(3) Å. Three-bonded nickel atoms (Ni(3b)) are connected to additional one-bonded

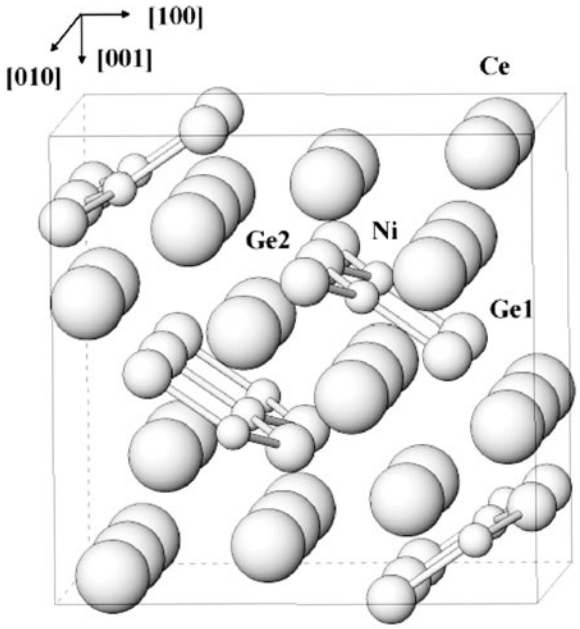

Figure 1. Crystal structure of Ce_3NiGe_2. The polyanions $[NiGe_2]$ are surrounded by cerium atoms forming trigonal prisms in two different orientations (vertical around Ge1 and horizontal around Ni and Ge2).

Table 1. Atomic coordinates and isotropic displacement parameters for Ce_3NiGe_2.

Atom	Site	x	y	z	B_{iso} (Å^2)
Ce1	4c	0.0578(2)	1/4	0.3759(2)	1.88(4)
Ce2	4c	0.2157(2)	1/4	0.7016(2)	2.01(5)
Ce3	4c	0.3813(2)	1/4	0.4410(2)	1.83(4)
Ni	4c	0.1275(4)	1/4	0.1340(4)	1.3(1)
Ge1	4c	0.3034(3)	1/4	0.0084(3)	2.42(9)
Ge2	4c	0.4745(3)	1/4	0.6859(3)	1.49(9)

germanium (Ge1(1b), d(Ni–Ge1) = 2.557(6) Å). Each atom of the polyanion is coordinated by six cerium atoms forming a trigonal prism with distances d(Ni–Ce) = 2.939–3.114 Å, d(Ge1–Ce) = 3.112–3.318 Å and d(Ge2–Ce) = 3.063–3.159 Å. The cerium atom distances to the ligands suggest the presence of $Ce^{3+}(4f^1)$ ions. Thus, the atomic environment and the interatomic distances in the polyanion can be described with a Zintl-like electron count $[Ce]_3^{3+}[Ge1(1b)]^{3-}[Ge2(2b)]^{2-}[Ni(3b)]^{3-}$ (assuming the Ni(II) valence state), giving only a slight access of electrons from the cations and suggesting herewith a metallic behaviour of the system.

The EDX analysis of the Ce-based sample yielded the composition Ce—53(1) at.%, Ni—15(1) at.%, Ge—32(1) at.%, that corresponds to the formula $Ce_{3.2(1)}Ni_{0.9(1)}Ge_{1.9(1)}$.

3.2. Magnetic properties

Figure 2 presents the temperature dependence of the inverse DC magnetic susceptibility for Ce_3NiGe_2. Above about 200 K the $\chi^{-1}(T)$ curve follows the Curie–Weiss law

$$\chi(T) = \frac{1}{8}\frac{\mu_{\text{eff}}^2}{T - \theta_{\text{p}}}, \tag{1}$$

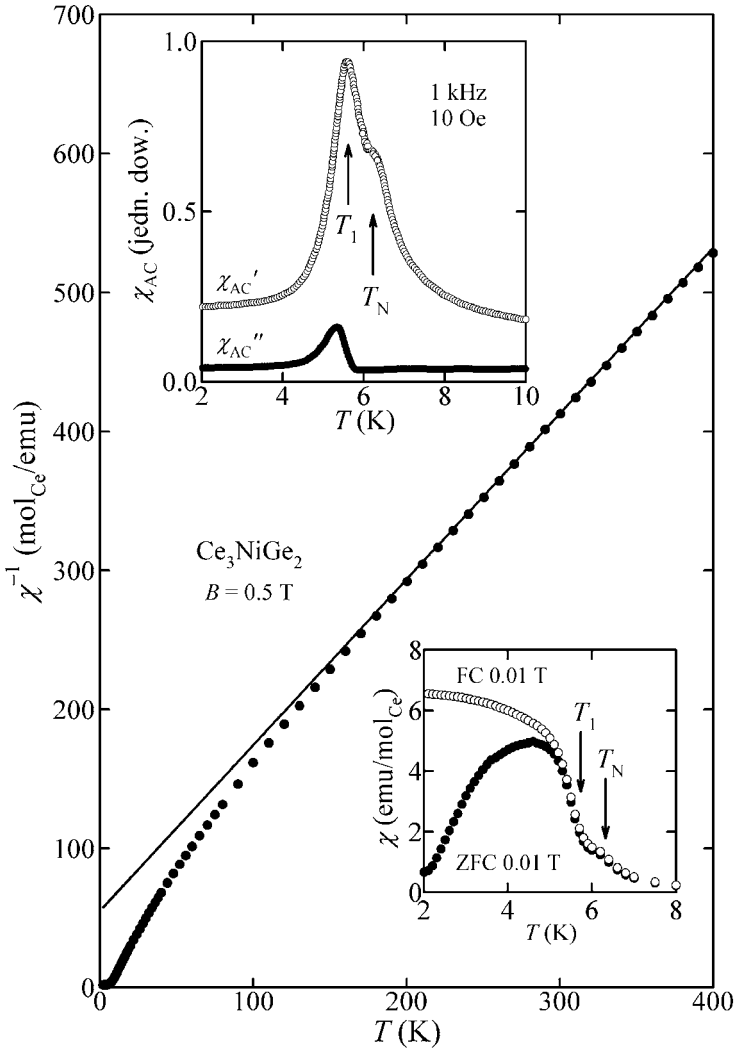

Figure 2. The inverse DC magnetic susceptibility of Ce_3NiGe_2. The solid line is a fit to equation (1). Lower inset: the low-temperature part of $\chi(T)$ taken in a weak magnetic field in ZFC and FC regimes. Upper inset: the real (χ'_{AC}) and imaginary (χ''_{AC}) parts of the AC magnetic susceptibility. The arrows indicate the magnetic phase transitions.

with the effective magnetic moment $\mu_{eff} = 2.59\ \mu_B$/Ce atom and the paramagnetic Curie temperature $\theta_p = -46$ K. The experimental value of μ_{eff} is close to the theoretical one calculated for a free Ce^{3+} ion ($\mu_{eff} = g\sqrt{j(j+1)} = 2.54\ \mu_B$). The strongly negative θ_p is indicative of antiferromagnetic exchange interactions and possibly of the Kondo effect (see below). At lower temperatures the $\chi^{-1}(T)$ curve deviates from a straight-line behaviour, presumably due to thermal depopulation of crystal–field levels.

As is apparent from the insets to figure 2, two subsequent magnetic phase transitions occur at $T_N = 6.2$ K and $T_1 = 5.2$ K. The upper one has an antiferromagnetic character, as manifested by the absence of any anomaly at T_N in the imaginary component of the AC susceptibility, as well as by fully reversible behaviour of the $\chi(T)$ curves measured around T_N in zero-field

cooling (ZFC) and field cooling (FC) regimes. In contrast, below T_1 the DC susceptibility measured in very weak fields shows a pronounced ferromagnetic-like irreversibility, whereas a sharp peak occurring at this temperature in $\chi'_{AC}(T)$ is accompanied by a clear structure in $\chi''_{AC}(T)$. These findings clearly indicate the ferromagnetic character of the ordering in Ce_3NiGe_2 at the lowest temperatures. It is also worth stressing that the low-temperature AC magnetic susceptibility is independent of amplitude and frequency of the probing field, hence excluding spin-glass phenomena.

The field dependence of the magnetization of Ce_3NiGe_2, measured at 2 K, is displayed in figure 3(a). The overall shape of $\sigma(B)$ corroborates the presumption of the ferromagnetic-like ground state. In low fields the magnetization rapidly increases with B, and above about 0.2 T it shows some tendency to saturation, reaching in a field of 5 T a value corresponding to the magnetic moment of 0.7 μ_B/Ce atom. This strong reduction of the cerium magnetic moment with respect to its free ion value of 2.14 μ_B can be ascribed to the concerted action of the crystal field and Kondo screening interactions. The $\sigma(B)$ curve exhibits a tiny hysteresis and rather small remanence of about 2.5 emu g^{-1}, both features being characteristic of soft ferromagnets. Accordingly, the low-temperature magnetization taken in a relatively weak field of 0.5 T (see the inset to figure 3(a)) does not show any difference while measured in ZFC and FC conditions.

Figure 3(b) presents the results of the Arrott scaling of the high-field parts of the $\sigma(B)$ curves, measured for Ce_3NiGe_2 at several temperatures above and below the ordering temperature. From the plot of B/σ versus σ^2 one estimates the Curie temperature in this compound as being equal to 5.1(1) K, in accordance with the value of T_1 derived from the AC and DC susceptibility data.

In contrast to the Ce-based compound, the magnetic susceptibility of La_3NiGe_2 is small and nearly independent of temperature, as expected for Pauli paramagnets.

3.3. Electrical properties

The temperature dependences of the electrical resistivity of Ce_3NiGe_2 and La_3NiGe_2 are shown in figure 4(a). The shape of the $\rho(T)$ curve measured for the latter compound has a metallic character and can be described by the modified Bloch–Grüneissen formula

$$\rho(T) = \rho_0 + 4R\Theta_R\left(\frac{T}{\Theta_R}\right)^5 \int_0^{\Theta_R/T} \frac{x^5\,dx}{(e^x - 1)(1 - e^{-x})} - KT^3, \qquad (2)$$

where ρ_0 is the temperature independent residual resistivity, the second term describes the electron–phonon scattering and the third term is a contribution due to the Mott-type s–d interband scattering. Least-squares fitting of the above function to the experimental data for La_3NiGe_2 yielded the following parameters: $\rho_0 = 36$ $\mu\Omega$ cm, $\Theta_R = 123$ K, $R = 0.72$ $\mu\Omega$ cm K^{-1} and $K = 19.4 \times 10^{-7}$ $\mu\Omega$ cm K^{-3}.

As is apparent from figure 4(a), the magnitude of the resistivity of Ce_3NiGe_2 is fairly large in the entire temperature range studied. With decreasing temperature it diminishes only slightly from the room-temperature value of about 400 $\mu\Omega$ cm down to about 330 $\mu\Omega$ cm at the minimum in $\rho(T)$ occurring around 30 K. At lower temperatures the $\rho(T)$ curve first shows an upturn, and then a sudden drop associated with the onset of the magnetic order at $T_N = 6.2$ K.

Assuming that the phonon contribution, ρ_{ph}, to the electrical resistivity of Ce_3NiGe_2 is properly approximated by ρ_{ph} of the isostructural La-based analogue, the magnetic contribution (enlarged by the residual resistivity) can be extracted from the total resistivity of Ce_3NiGe_2 in

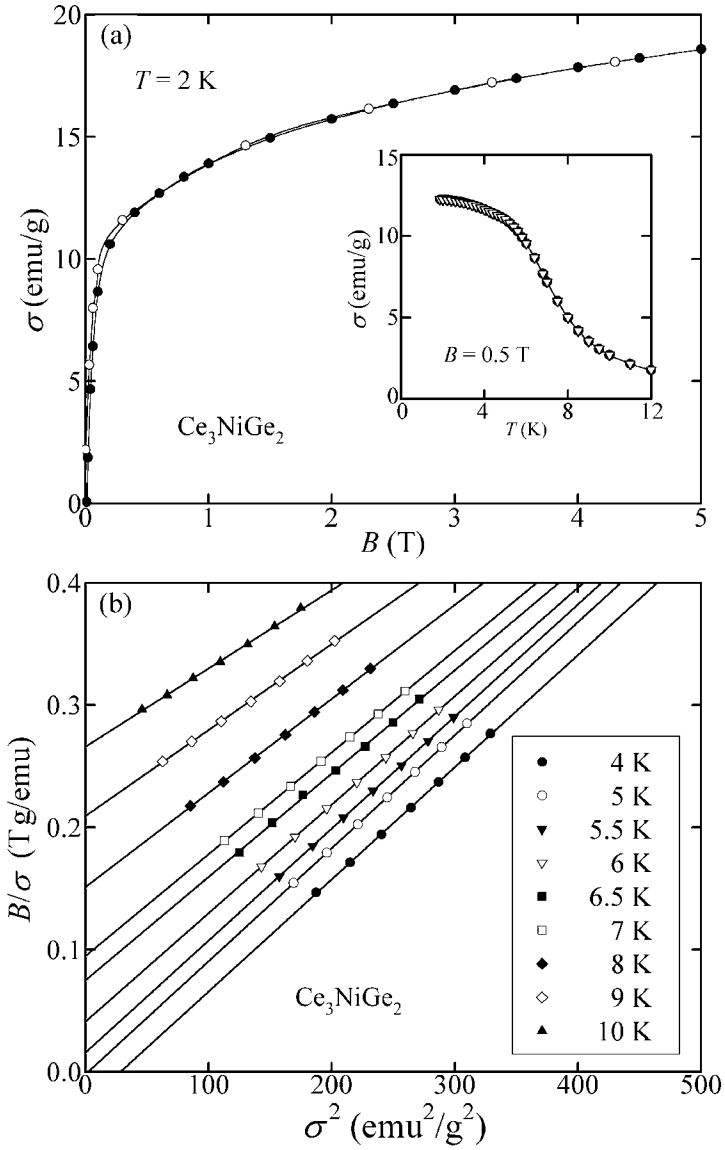

Figure 3. (a) The field dependence of the magnetization of Ce_3NiGe_2 measured with increasing (closed circles) and decreasing (open circles) magnetic field. The solid curve serves as a guide for the eye. Inset: the temperature variation of the magnetization measured in ZFC and FC regimes (circles and triangles, respectively) in a magnetic field of 0.5 T. (b) The Arrott plots of the magnetization taken at various temperatures.

the following manner:

$$\rho_{\mathrm{mag}}(Ce_3NiGe_2) + \rho_0(Ce_3NiGe_2) = \rho(Ce_3NiGe_2) - \underbrace{(\rho(La_3NiGe_2) - \rho_0(La_3NiGe_2))}_{\rho_{\mathrm{ph}}}. \quad (3)$$

Figure 4(b) displays the so-obtained temperature variation of $\rho_{\mathrm{mag}} + \rho_0$ of Ce_3NiGe_2 in a semi-logarithmic scale. The main finding is here the presence of two temperature intervals in which resistivity decreases logarithmically: 10–35 K and above 150 K. According to Cornut

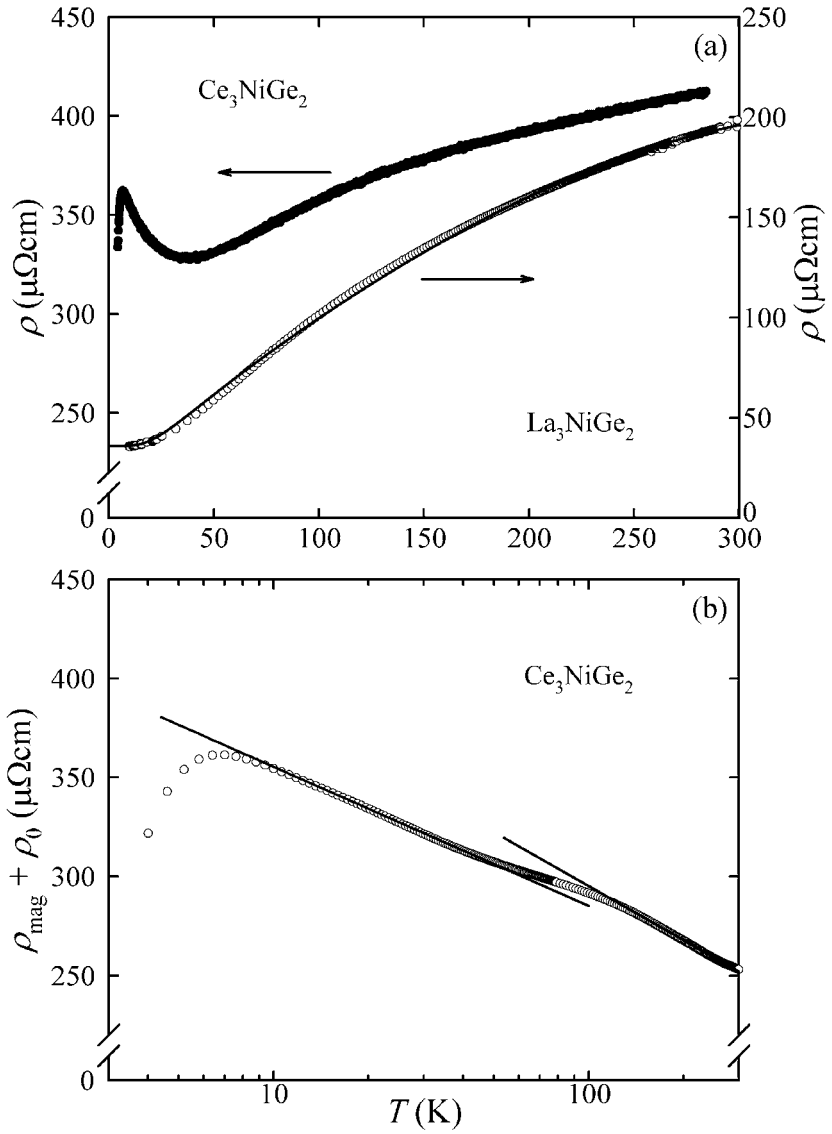

Figure 4. (a) The temperature variation of the electrical resistivity of Ce_3NiGe_2 and La_3NiGe_2. The solid curve is a fit of the data for La_3NiGe_2 to equation (2). (b) The magnetic contribution to the resistivity of Ce_3NiGe_2. The solid lines are fits to equation (4).

and Coqblin [16], such a behaviour arises due to Kondo scattering of conduction electrons on magnetic moments in systems exhibiting crystal field interactions. The least-squares fitting of the experimental data to the function

$$\rho_{\mathrm{mag}}(T) = \rho_0^{\infty} - c_{\mathrm{K}} \ln T, \tag{4}$$

where ρ_0^{∞} is the temperature independent spin-disorder resistivity and c_{K} is the Kondo coefficient, yielded the following parameters: $\rho_0^{\infty} + \rho_0 = 426\ \mu\Omega$ cm and $c_{\mathrm{K}} = 31\ \mu\Omega$ cm for the low-temperature slope, and $\rho_0^{\infty} + \rho_0 = 476\ \mu\Omega$ cm and $c_{\mathrm{K}} = 39\ \mu\Omega$ cm for the high-temperature slope. The closeness of the respective values obtained for the two temperature

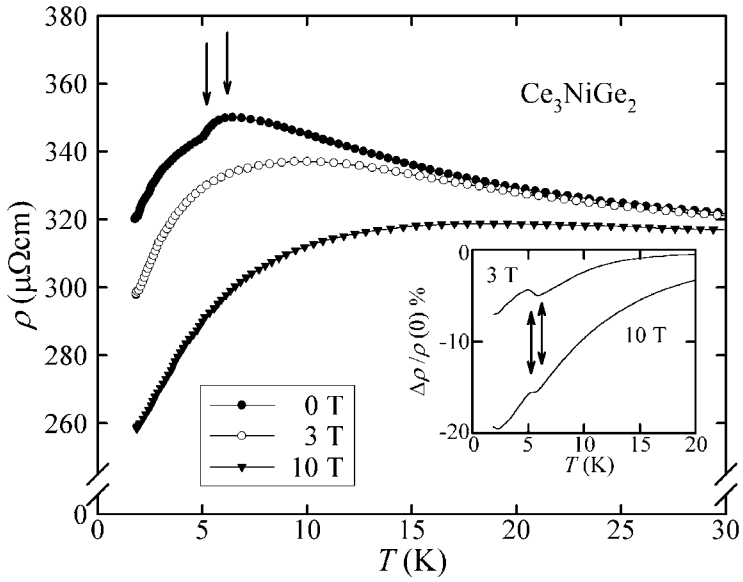

Figure 5. The electrical resistivity of Ce_3NiGe_2 versus temperature, measured in a magnetic field of 0, 3 and 10 T. Inset: the temperature dependence of the magnetoresistivity. The arrows mark the magnetic phase transitions.

regions suggests that the observed $\rho \sim -\ln T$ dependences may result from Kondo scattering of the conduction electrons on the same level, i.e. on the ground doublet, thus implying that the first excited doublet lies at least 300 K above the ground level. The origin of the crossover from the high-temperature log-T behaviour to the lower one is unknown. The electrical resistivity data are thus at this point rather inconsistent with the results of the specific heat analysis (see below).

The temperature dependence of the electrical resistivity of Ce_3NiGe_2 taken in several applied magnetic fields is shown in figure 5. The resistivity gradually decreases with increasing magnetic field, as one expects for Kondo systems. The magnetoresistivity (MR) defined as $\Delta\rho/\rho(0) = (\rho(B) - \rho(B = 0))/\rho(B = 0)$ is negative and its absolute value attains in a field of 10 T at $T = 1.5$ K a value of about 20% (see the inset to figure 5). Obviously, the magnetic phase transitions in Ce_3NiGe_2 are well recognizable on the MR curves even if they are hardly seen on $\rho(T)$ taken in high magnetic fields.

Figure 6(a) displays the field dependence of MR measured at several temperatures from the ordered and paramagnetic regions. The magnetoresistivity is always negative in the entire magnetic field range studied. At the lowest temperatures (1.8 K) MR reaches a value of about -26% in a field 14 T. As shown in figure 6(b), the MR isotherms taken in the paramagnetic state can be nearly superimposed onto each other by plotting $\Delta\rho/\rho(0)$ as a function of $B/(T + T^*)$, where $T^* = -4$ K is a scaling parameter. Though the single-ion Kondo scaling [17] implies positive values of the characteristic temperature, which is directly related to the strength of Kondo interactions, one should note that negative values of T^* have also been determined, e.g. for an archetypal heavy-fermion system UBe_{13} [18], and interpreted as being due to the presence of ferromagnetic correlations. It is clear that ferromagnetic exchange interactions are also effective in Ce_3NiGe_2, that shows ferromagnetic-like ordering at low temperatures. The ferromagnetic character of the magnetic order may be corroborated by the negative values of $\Delta\rho/\rho$ as well.

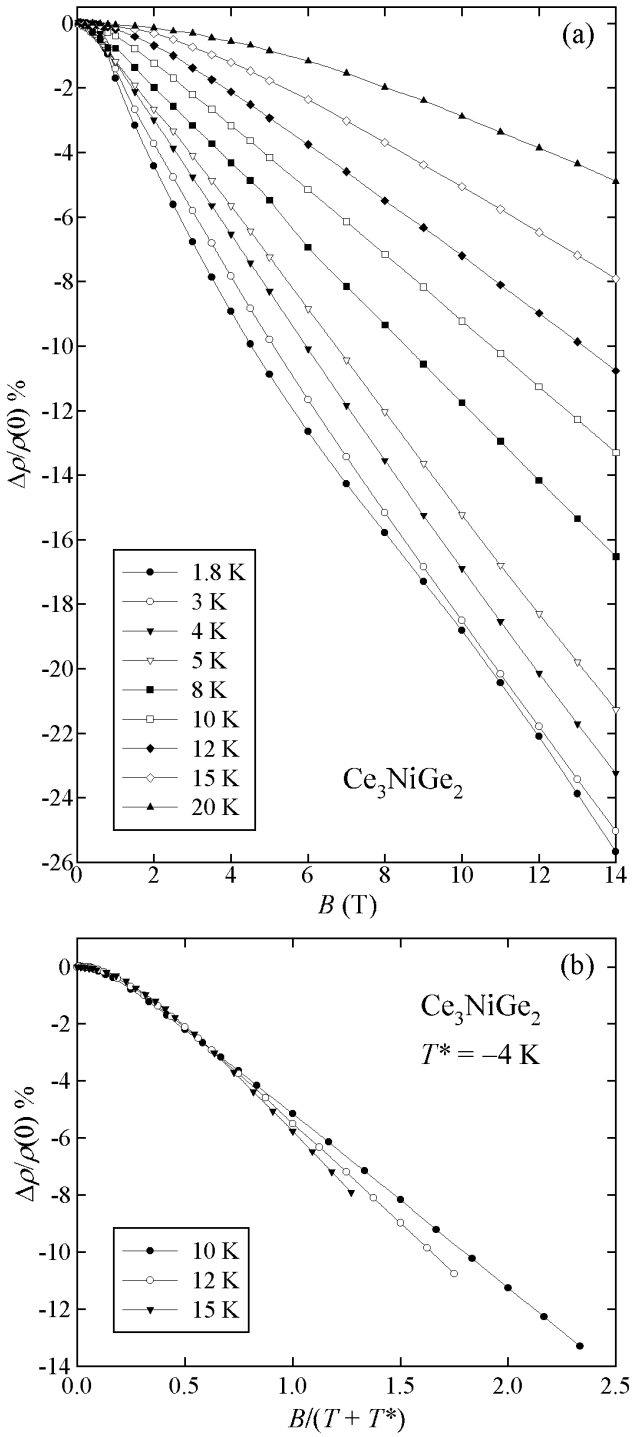

Figure 6. (a) The field dependence of the magnetoresistivity of Ce_3NiGe_2 measured at several different temperatures. (b) The Schlottman scaling of the $\Delta\rho/\rho(0)$ curves taken in the paramagnetic region.

3.4. Thermodynamic properties

In figure 7(a) there are presented the temperature dependences of the specific heat of Ce_3NiGe_2 and La_3NiGe_2. $C_p(T)$ of the La-based phase has a character typical for non-magnetic metals. As seen from the inset to figure 7(a), the temperature variation of its specific heat can be described below about 7 K by the formula

$$C_p(T) = \gamma T + \beta T^3 \tag{5}$$

with the fitting parameters $\gamma = 5.4$ mJ $\text{mol}_{\text{La}}^{-1}$ K^{-2} and $\beta = 10.1 \times 10^{-4}$ mJ $\text{mol}_{\text{La}}^{-1}$ K^{-4}. The characteristic temperature Θ_{D}, calculated from β, is about 226 K. Both parameters (the Sommerfeld coefficient γ and the Debye temperature Θ_{D}) have values typical for nonmagnetic intermetallic compounds. In contrast, $C_p(T)$ of Ce_3NiGe_2 manifests its magnetic character—a double λ-shaped anomaly is superimposed on the sigmoid-like curve marking the magnetic phase transitions at the temperatures $T_{\text{N}} = 6.2$ K and $T_{\text{l}} = 5.2$ K (see also figure 7(c)).

Assuming that the phonon contribution to C_p of La_3NiGe_2 describes well the corresponding contribution to the specific heat of Ce_3NiGe_2, the magnetic contribution to C_p of the latter compound (enlarged by the electronic term C_{el}) can be estimated as

$$\Delta C = C_p(\text{Ce}_3\text{NiGe}_2) - \underbrace{(C_p(\text{La}_3\text{NiGe}_2) - C_{\text{el}}(\text{La}_3\text{NiGe}_2))}_{\approx C_{\text{ph}}}. \tag{6}$$

The so-obtained temperature variation of ΔC is presented in figure 7(b). In the paramagnetic region this dependence can be described by the sum of the regular electronic term $C_{\text{el}} = \gamma_p T$ (with the value $\gamma_p = 5.4$ mJ $\text{mol}_{\text{La}}^{-1}$ K^{-2} found for the La-based counterpart), the Kondo specific heat C_{K} (calculated as given in [19]) and the Schottky contribution C_{Sch} due to the crystal field effect. In the case of Ce_3NiGe_2, Ce^{3+} ions experience noncubic crystal–field potential and thus the sixfold degenerate $^2F_{5/2}$ ground multiplet splits into three doublets with energy separations Δ_1 and Δ_2. The least-squares fitting procedure yielded the following parameters: $T_{\text{K}} = 37$ K, $\Delta_1 = 330$ K and $\Delta_2 = 690$ K.

The assumed scheme of the crystal–field splitting (2:2:2) together with the values of Δ_1 and Δ_2 are consistent with the results of the analysis of the magnetic susceptibility and electrical resistivity of Ce_3NiGe_2. As shown by Mulak [20], the population of the excited crystal–field levels becomes effective at temperatures higher than $\Delta_n/3$. Thus, the Curie–Weiss behaviour of the magnetic susceptibility, with μ_{eff} close to the free Ce^{3+} ion value, is here observed only at temperatures higher than about $\Delta_2/3 = 690/3 = 230$ K (figure 2). In turn, the high value of Δ_1 explains the absence of any clear maximum in $\rho_{\text{mag}}(T)$, characteristic of the interplay of Kondo and crystal–field interactions. It is also worth noting that the magnetic entropy in Ce_3NiGe_2 achieves at 140 K a value of only $1.95R\ln 2$ (figure 7(b)), implying that at this temperature the second excited doublet is hardly populated, and hence its energy is larger than 3×140 K $= 420$ K.

An independent estimate for the Kondo temperature in Ce_3NiGe_2 is provided by the method developed by Blanco *et al* [21] and Yashima *et al* [22]. These authors derived the formulae describing the specific heat jump δC and the magnetic entropy S, respectively, at the ordering temperature in a Kondo system:

$$\delta C\left(-\frac{T_{\text{K}}}{T_{\text{N}}}\right) = \frac{6k_{\text{B}}}{\psi'''(\frac{1}{2}+\zeta)}\left[\psi'\left(\frac{1}{2}+\zeta\right) + \zeta\psi''\left(\frac{1}{2}+\zeta\right)\right]^2, \tag{7}$$

$$S\left(-\frac{T_{\text{K}}}{T_{\text{N}}}\right) = R\left[\ln\left(1+\exp\left(-\frac{T_{\text{K}}}{T_{\text{N}}}\right)\right) + \frac{T_{\text{K}}}{T_{\text{N}}}\frac{\exp(-\frac{T_{\text{K}}}{T_{\text{N}}})}{1+\exp(-\frac{T_{\text{K}}}{T_{\text{N}}})}\right], \tag{8}$$

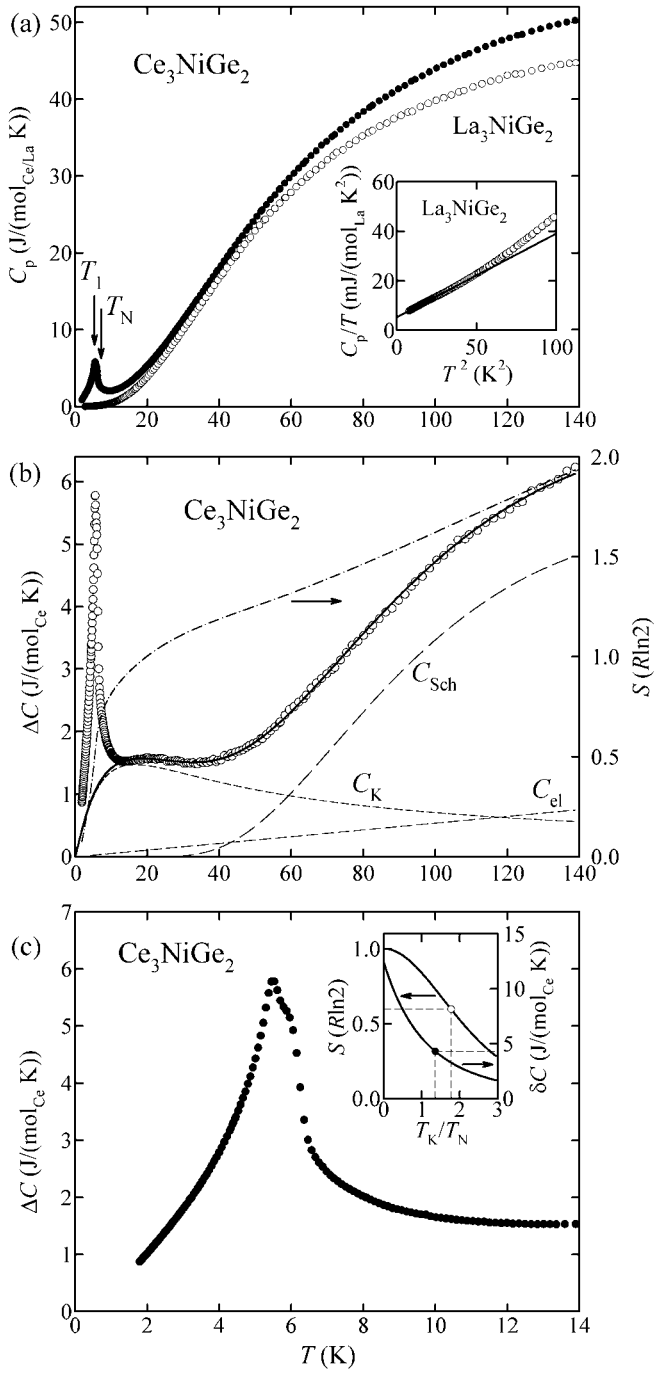

Figure 7. (a) The specific heat of Ce_3NiGe_2 and La_3NiGe_2 versus temperature. The arrows mark the magnetic phase transitions. Inset: C_p/T versus T^2 for the La compound—the solid curve is a fit to equation (5). (b) The non-lattice specific heat and the magnetic entropy (dash–dotted curve) versus temperature (left- and right-hand axes, respectively). The solid curve is a fit to the sum of the electronic and Kondo contributions (see the text), plotted separately as the dashed curves. (c) The temperature dependence of the non-lattice specific heat in the vicinity of the magnetic phase transitions. Inset: the estimation of the Kondo temperature according to equations (7) and (8).

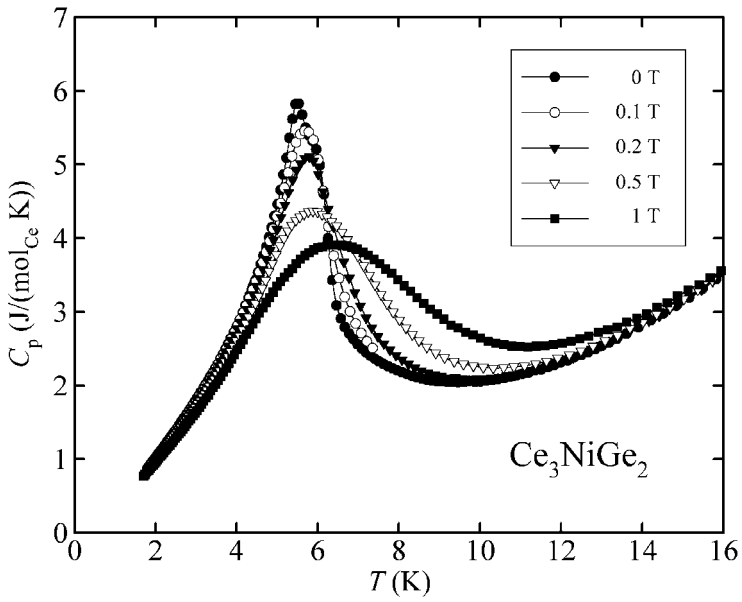

Figure 8. The temperature variation of the specific heat of Ce_3NiGe_2 taken in applied magnetic fields.

where $\zeta = (T_K/T_N)/2\pi$ and ψ', ψ'' and ψ''' are the first three derivatives of the digamma function. As can be inferred from figures 7(b) and (c), the specific heat jump due to the magnetic ordering in Ce_3NiGe_2, being about 4.2 J mol_{Ce}^{-1} K^{-1}, is much lower than the value of 12.48 J mol_{Ce}^{-1} K^{-1} expected for a system with doublet ground state and no Kondo effect. Also the magnetic entropy at T_N is strongly reduced and amounts to only $0.64R \ln 2$ (note the right-hand axis). Thus, analysing the experimental data in terms of equations (7) and (8) (see the graphical representation in the inset to figure 7(c)), one obtains $T_K = 8.4$ and 10, respectively. It is worth emphasizing the internal consistency of these two estimates, which are however considerably smaller than the value derived above from the non-lattice contribution ΔC to the specific heat in the paramagnetic region ($T_K = 37$ K). According to Desgranges and Rasul [23], this discrepancy probably results from the oversimplification made in the analysis of ΔC by assuming that the Kondo and Schottky terms in $\Delta C(T)$ are just additive.

Finally, figure 8 displays the evolution of the specific heat of Ce_3NiGe_2 upon applying external magnetic field. As seen, with increasing field the λ-shaped peak continuously diminishes, broadens and shifts towards higher temperatures. Such a behaviour of the specific heat is characteristic of ferromagnets. Worth noting is that for Ce_3NiGe_2 appreciable changes in $C_p(T)$ are observed already in relatively weak magnetic fields.

3.5. Electronic density of states for Ce_3NiGe_2

The electronic structure of Ce_3NiGe_2 was calculated using the local density functional approach (LDA) as implemented in the tight-binding-LMTO program package of Andersen *et al* [24] with exchange–correlation potential according to Barth and Hedin [25]. The radial scalar-relativistic Dirac equation was solved to get the partial waves. The calculations within the atomic sphere approximation (ASA) included corrections due to neglecting the interstitial regions and the partial waves of higher order [26]. It appeared however that the interstitial

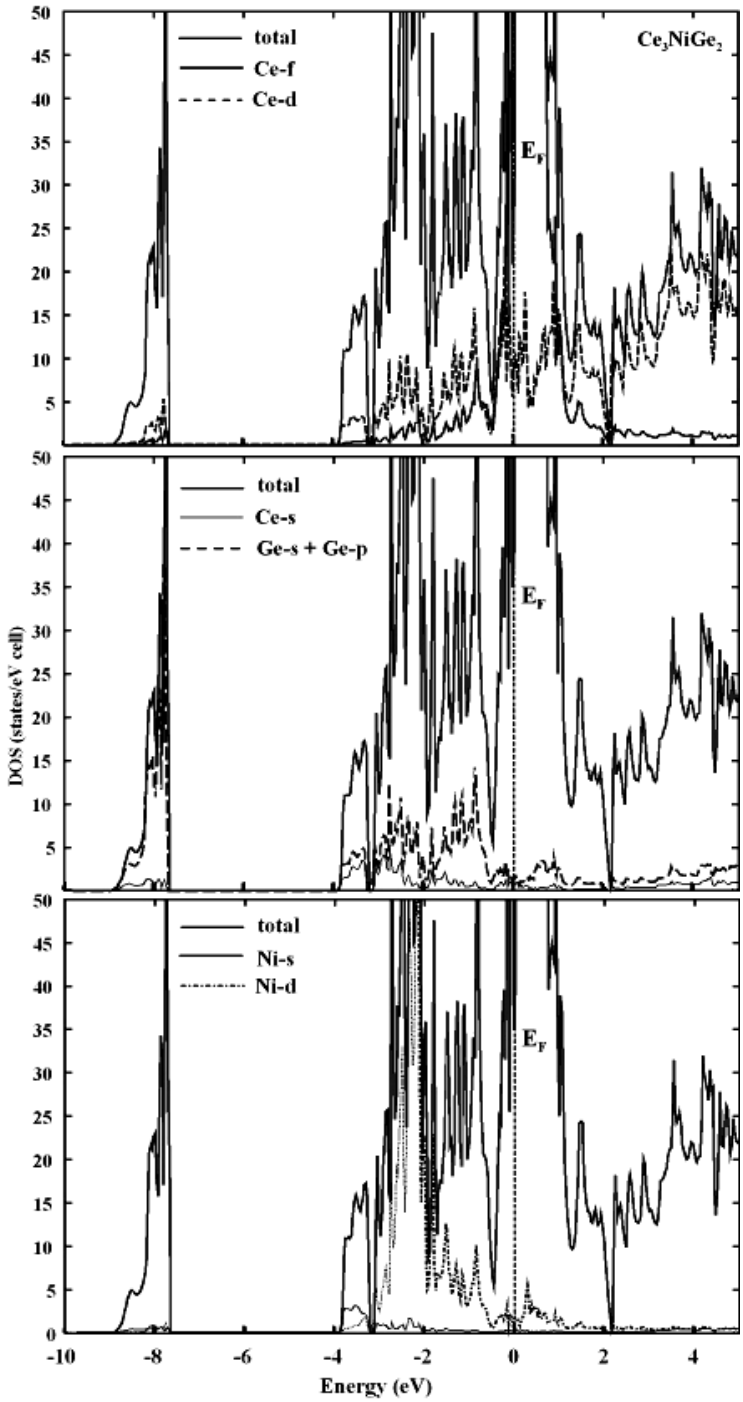

Figure 9. Electronic density of states for Ce_3NiGe_2 with partial contributions of the components dominating in the region near the Fermi level (top) and in the valence region (middle and bottom).

spheres (E), usually added to reduce the overlap of the atomic spheres, were not necessary in the case of Ce_3NiGe_2.

The total density of states (DOS) for Ce_3NiGe_2 together with partial contributions of different components is presented in figure 9. The DOS near the Fermi level is very high, reflecting a metallic character of Ce_3NiGe_2. It is mainly governed by the Ce 4f and 5d states, that hybridize with the Ni 3d states. The resulting bands are strongly extended at energies higher than -4 eV. The Ni 3d band mainly defines the upper part of the valence zone (from -3 to -0.5 eV) with the main peak located about 2 eV below E_F (figure 9, top). The lower part of the valence zone is formed by Ni 4s, Ge 4s and Ge 4d states with some contributions from the Ce 6s states (figure 9, bottom). This finding agrees well with the simple picture of the Zintl-like electron count, derived from the crystallographic data (see section 3.1). As expected from this count, the s and p electrons of germanium form the bonds together with the s electrons of nickel and cerium with little contribution of 5d and 4f electrons of cerium.

4. Summary

The collected experimental data show Ce_3NiGe_2 to be a dense Kondo system with the Kondo temperature of the order of 10 K and the total crystal–field splitting of about 690 K. The compound orders magnetically at low temperatures, and the magnetic ground state has a ferromagnetic-like nature as inferred from characteristic behaviour of the AC and DC magnetic susceptibility as a function of temperature and magnetic field as well as from the field dependences of the resistivity and the specific heat. However, as found in the recent neutron powder diffraction study [12], Ce_3NiGe_2 is not a simple ferromagnet but shows at 1.4 K a complex magnetic structure of ferrimagnetic type. In the present paper we argue that this spin arrangement transforms at $T_1 = 5.2$ K into a compensated antiferromagnetic structure, before entering the paramagnetic state at $T_N = 6.2$ K. A neutron diffraction experiment is planned to prove this hypothesis and to determine the magnetic structure of Ce_3NiGe_2 in between T_1 and T_N.

Acknowledgments

The authors are grateful to Professor A Czopnik, Dr V H Tran and Dr A Zaleski for help in specific heat, magnetoresistivity and AC magnetic susceptibility measurements, respectively. The work was supported by the Polish State Committee of Scientific Research KBN (grant No 2 P03B 028 23), the Austrian–Polish Scientific–Technical Exchange Programme (project No 15/2003) and the Max-Planck-Gesellschaft (research fellowships for APP and DK).

References

[1] Lister S J S, Grosche F M, Carter F V, Haselwimmer R K W, Saxena S S, Mathur N D, Julian S R and Lonzarich G G 1997 *Z. Phys.* B **103** 263
[2] Grosche F M, Agarwal P, Julian S R, Wilson N J, Haselwimmer R K W, Lister S J S, Mathur N D, Carter F V, Saxena S S and Lonzarich G G 2000 *J. Phys.: Condens. Matter* **12** L533
[3] Pecharsky V K, Gschneidner K A Jr and Miller L L 1991 *Phys. Rev.* B **43** 10906
[4] Geibel C, Kämmerer C, Seidel B, Bredl C D, Grauel A and Steglich F 1992 *J. Magn. Magn. Mater.* **108** 207
[5] Jung M H, Harrison N, Lacerda A H, Nakotte H, Pagliuso P G, Sarrao J L and Thompson J D 2002 *Phys. Rev.* B **66** 054420
[6] Pikul A P, Kaczorowski D, Plackowski T, Czopnik A, Michor H, Bauer E, Hilscher G, Rogl P and Grin Yu 2003 *Phys. Rev.* B **67** 224417

[7] Durivault L, Bourée F, Chevalier B, André G, Weill F, Etourneau J, Martinez-Samper P, Rodrigo J G, Suderow H and Vieira S 2003 *J. Phys.: Condens. Matter* **15** 77
[8] Hossain Z, Hamashima S, Umeo K, Takabatake T, Geibel C and Steglich F 2000 *Phys. Rev.* B **62** 8950
[9] Pikul A P, Kaczorowski D and Rogl P 2002 *Physica* B **312/313** 422
[10] Pikul A P, Kaczorowski D, Rogl P and Grin Yu 2003 *Phys. Status Solidi* b **236** 364
[11] Pikul A P, Kaczorowski D, Michor H, Rogl P, Czopnik A, Grin Yu, Bauer E and Hilscher G 2003 *Acta Phys. Pol.* B **34** 1235
[12] Durivault L 2002 *Thesis* L'Universite Bordeaux 1, unpublished
[13] Salamakha P, Konyk M, Sologub O and Bodak O 1996 *J. Alloys Compounds* **236** 206
[14] Bodak O I, Bruskov V A and Pecharsky V K 1982 *Kristallographiya* **27** 896
[15] Rodriguez-Carvajal J 1992 *Physica* B **192** 55
[16] Cornut D and Coqblin B 1972 *Phys. Rev.* B **5** 4541
[17] Schlottmann P 1989 *Phys. Rep.* **181** 1
[18] Andraka B and Stewart G R 1994 *Phys. Rev.* B **49** 12359
[19] Desgranges H U and Schotte K D 1982 *Phys. Lett.* A **91** 240
[20] Mulak J 1986 *J. Less-Common Met.* **121** 141
[21] Blanco J A, de Podesta M, Espeso J I, Gómez Sal J C, Lester C, McEwen K A, Patrikios N and Rodríguez Fernández J 1994 *Phys. Rev.* B **49** 15126
[22] Yashima H, Mori H, Sato N, Satoh T and Kohn K 1983 *J. Magn. Magn. Mater.* **31–34** 411
[23] Desgranges H U and Rasul J W 1985 *Phys. Rev.* B **32** 6100
[24] Jepsen O, Burkhardt A and Andersen O K 1999 *The Program TB–LMTO–ASA. Version 4.7* (Stuttgart: Max-Planck-Institut für Festkörperforschung)
[25] Barth U and Hedin L 1972 *J. Phys. C: Solid State Phys.* **5** 1629
[26] Andersen O K, Pawlowska Z and Jepsen O 1986 *Phys. Rev.* B **34** 5253